

PAPER • OPEN ACCESS

Dose rate determination for preclinical total body irradiation

To cite this article: Yuncheng Zhong *et al* 2020 *Phys. Med. Biol.* **65** 175018

View the [article online](#) for updates and enhancements.

You may also like

- [3D cell-printing of tendon-bone interface using tissue-derived extracellular matrix bioinks for chronic rotator cuff repair](#)
Suhun Chae, Yucheng Sun, Yeong-Jin Choi *et al.*
- [Review of wearable technologies and machine learning methodologies for systematic detection of mild traumatic brain injuries](#)
William Schmid, Yingying Fan, Taiyun Chi *et al.*
- [Recent advances in medical countermeasure development against acute radiation exposure based on the US FDA animal rule](#)
Thomas J MacVittie and Ann M Farese



JOIN US | ESTRO 2024
**In-Booth Talks, Demos,
& Lunch Symposium**

[Browse talk schedule >](#)

SUN NUCLEAR
A MEDTRONIC MEDICAL COMPANY



PAPER

Dose rate determination for preclinical total body irradiation

OPEN ACCESS

Yuncheng Zhong^{1,2}, Youfang Lai^{1,2,3}, Debabrata Saha¹, Michael D Story¹, Xun Jia^{1,2} and Strahinja Stojadinovic¹ RECEIVED
25 April 2020REVISED
23 June 2020ACCEPTED FOR PUBLICATION
8 July 2020PUBLISHED
4 September 2020¹ Department of Radiation Oncology, University of Texas Southwestern Medical Center, Dallas, TX 75287, United States of America² Innovative Technologies Of Radiotherapy Computations and Hardware (iTORCH) Laboratory, Department of Radiation Oncology, University of Texas Southwestern Medical Center, Dallas, TX 75287, United States of America³ Department of Physics, University of Texas at Arlington, Arlington, TX 76019, United States of AmericaE-mail: Strahinja.Stojadinovic@UTsouthwestern.edu and Xun.Jia@UTsouthwestern.edu**Keywords:** total body irradiation, small animal irradiation, radiobiology dosimetry

Original content from this work may be used under the terms of the [Creative Commons Attribution 3.0 licence](https://creativecommons.org/licenses/by/4.0/). Any further distribution of this work must maintain attribution to the author(s) and the title of the work, journal citation and DOI.

**Abstract**

The accuracy of delivered radiation dose and the reproducibility of employed radiotherapy methods are key factors for preclinical radiobiology applications and research studies. In this work, ionization chamber (IC) measurements and Monte Carlo (MC) simulations were used to accurately determine the dose rate for total body irradiation (TBI), a classic radiobiologic and immunologic experimental method. Several phantom configurations, including large solid water slab, small water box and rodentomorphic mouse and rat phantoms were simulated and measured for TBI setup utilizing a preclinical irradiator XRad320. The irradiator calibration and the phantom measurements were performed using an ADCL calibrated IC N31010 following the AAPM TG-61 protocol. The MC simulations were carried out using Geant4/GATE to compute absorbed dose distributions for all phantom configurations. All simulated and measured geometries had favorable agreement. On average, the relative dose rate difference was 2.3%. However, the study indicated large dose rate deviations, if calibration conditions are assumed for a given experimental setup as commonly done for a quick determination of irradiation times utilizing lookup tables and hand calculations. In a TBI setting, the reference calibration geometry at an extended source-to-surface distance and a large reference field size is likely to overestimate true photon scatter. Consequently, the measured and hand calculated dose rates, for TBI geometries in this study, had large discrepancies: 16% for a large solid water slab, 27% for a small water box, and 31%, 36%, and 30% for mouse phantom, rat phantom, and mouse phantom in a pie cage, respectively. Small changes in TBI experimental setup could result in large dose rate variations. MC simulations and the corresponding measurements specific to a designed experimental setup are vital for accurate preclinical dosimetry and reproducibility of radiobiological findings. This study supports the well-recognized need for physics consultation for all radiobiological investigations.

1. Introduction

The accuracy of delivered radiation dose and the reproducibility of employed radiotherapy methods are key factors for preclinical radiobiology applications and research studies. The prerequisite for accurate evaluation of dose and dose uncertainty is traceability to the reference radiation standard. In the U.S., the standard is determined and maintained by the National Institute of Standards and Technology (NIST) or by the Accredited Dosimetry Calibration Laboratories (ADCLs). NIST or ADCLs calibrated dosimetry equipment ensures that there is a documented unbroken link to the reference standard which provides known dose uncertainty under calibration conditions. A variety of different dosimetry protocols are available for irradiator calibrations depending on the type (gamma rays, x-rays, charged particles) and energy (kV, MV) of the radiation source. Superficial and orthovoltage x-ray energies are predominantly utilized in contemporary commercial small animal irradiation platforms. The American Association of Physicists in Medicine (AAPM) published a guidance document, developed by Radiation Therapy Committee Task Group

61 (TG-61), with recommendations for 40–300 kV x-ray beam reference dosimetry. NIST traceability and a properly calibrated irradiator, however, only provide a good starting point. The ultimate goal is to determine dose and the corresponding dose uncertainty for any given irradiation setup which is likely to be different from calibration conditions.

Radiation dose is more than a number (Desrosiers *et al* 2013) as many factors may impact the intended dose distribution. Key factors for dose calculations include reference output at the calibration point, distance from the source, dose falloff as a function of depth and attenuation of the medium, radiation field size (FS), the presence of beam modifiers such as filters and lab equipment used to aid the experiments, etc. In addition, somewhat less obvious dose variables include objects and materials beyond the irradiated target, dose rate variations, walls and components of self-shielded irradiator systems, the number of interfaces between different media, etc. These factors in conjunction with a given experimental geometry may not ensure charged particle equilibrium, a fundamental requirement necessary for accurate measurements.

In practice, the aforementioned considerations are neither trivial nor easy and present traps for remarkable dosimetric fails. An expert panel consensus document (Desrosiers *et al* 2013), emphasizing the importance of dosimetry standardization in radiobiology studies and reporting dosimetry details in research articles, was published as a result of the workshop hosted in 2011 by the National Cancer Institute (NCI), the National Institute of Allergy and Infectious Diseases (NIAID), and the National Institute of Standards and Technology (NIST). Publications without crucial dosimetry information clutter valid scientific findings with results difficult or impossible to reproduce and compare with similar studies. A study analyzing radiobiology publications in last 20 years found that highly cited journals and articles are systematically more likely to be lacking dosimetry details related to irradiation protocols and that such practice may have contributed to the data interpretation and reproducibility crisis (Draeger *et al* 2020).

There is an increasing body of publications (Lindsay *et al* 2014, Pedersen *et al* 2016, Seed *et al* 2016) with documented large dose discrepancies in radiobiology studies indicating that physics consultation should not only be recommended, rather it should be mandated as in-depth physics expertise is crucial for accurate dose calculations (Deng *et al* 2007, Wong *et al* 2008, Tryggestad *et al* 2009, Chow *et al* 2010, Yoshizumi *et al* 2011, Pidikiti *et al* 2011, Clarkson *et al* 2011, Newton *et al* 2011, Hoof *et al* van 2013, Noblet *et al* 2016, Na *et al* 2018, Soultanidis *et al* 2019, Vaniqui *et al* 2019). This manuscript exemplifies such a necessity for one of the most commonly used experimental methods, total body irradiation (TBI), still commonly utilized in contemporary studies of radiobiology and immunology.

2. Methods and materials

A commercial small animal irradiator, XRad 320 (PXI, North Branford, CT), is regularly used by numerous research labs for a variety of radiobiological experiments at UT Southwestern Medical Center in Dallas. The objective of this study was to determine accurate dose rate for a whole-body small animal irradiation setup utilizing the XRad 320 platform.

2.1. Instrumentation

The XRad 320 platform is a self-shielded irradiation system with a fixed gantry MXR-321 x-ray tube (Comet AG, Liebefeld-Berne, Switzerland). The variable tube current (0.1 to 45 mA) and tube potential (5 to 320 kVp) provide a valuable range of orthovoltage photon energies. The tube has an inherent filtration of 3 mm Be and an added filtration of 1.65 mm Al. For a 250 kVp tube potential and 15 mAs tube current the measured half-value layer (HVL) was 0.45 mm Cu (Pidikiti *et al* 2011). The system is equipped with a motorized adjustable collimator. The collimator is used to define rectangular FSs (min FS $0.95 \times 0.15 \text{ cm}^2$, max FS $26.4 \times 26.4 \text{ cm}^2$) projected on top of detachable 3 mm thick steel plate at a 65.0 cm distance from the x-ray focal spot. The experimental configurations are illustrated in figure 1.

A PTW UNIDOS E electrometer and N31010 ionization chamber (PTW North America Corporation, New York, NY) were calibrated by the ADCL at the University of Wisconsin. The UW250-M beam quality was requested for the ionization chamber calibration. The corresponding air-kerma calibration coefficient N_K was $2.774 \times 10^8 \text{ Gy/C}$. The electrometer charge calibration coefficients for low, medium and high settings were, $1.000 \text{ pC Rdg}^{-1}$, $0.997 \text{ pC Rdg}^{-1}$, $1.000 \text{ pC Rdg}^{-1}$, respectively. Throughout measurements, the atmospheric pressure was monitored using a digital barometer (Fisherbrand, Fisher Scientific, Pittsburgh, PA) and the temperature by a thermal gauge (Fisherbrand Durac Plus, Fisher Scientific, Pittsburgh, PA).

A 1D-scanner water tank (Sun Nuclear Corporation, Melbourne, FL) was utilized for the in-air measurements (figure 1(a)). The 1D scanner consists of an acrylic box, a detector holder and a linear translational stage to control the vertical position of the ionization chamber. The acrylic box has $35.0 \times 39.0 \times 36.2 \text{ cm}^3$ inner and $37.6 \times 40.6 \times 36.8 \text{ cm}^3$ outer dimensions with a maximum scanning depth of 30 cm.

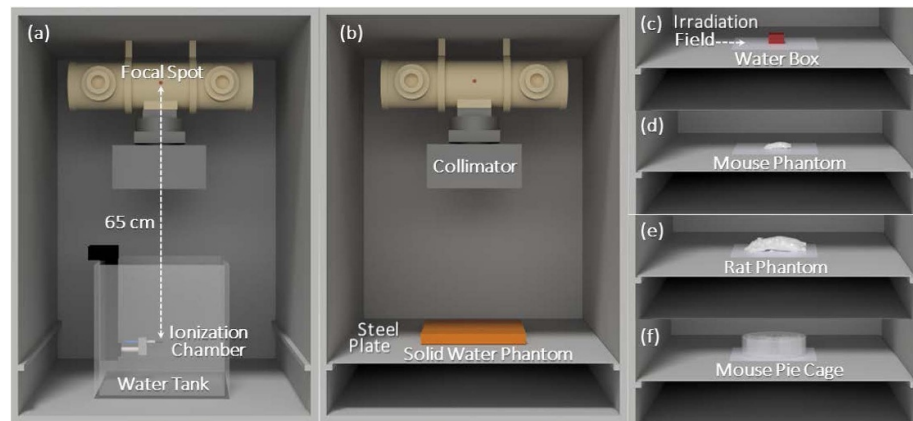


Figure 1. The configurations used for dose measurements. (a) In-air calibration setup; (b) the solid water phantom; (c) the small water box phantom; (d) the silicon rubber mouse phantom; (e) the silicon rubber rat phantom; (f) the mouse pie cage. Fully opened collimator with the maximum irradiation field, $26.4 \times 26.4 \text{ cm}^2$, projected on the steel plate at a 65 cm focal spot distance.

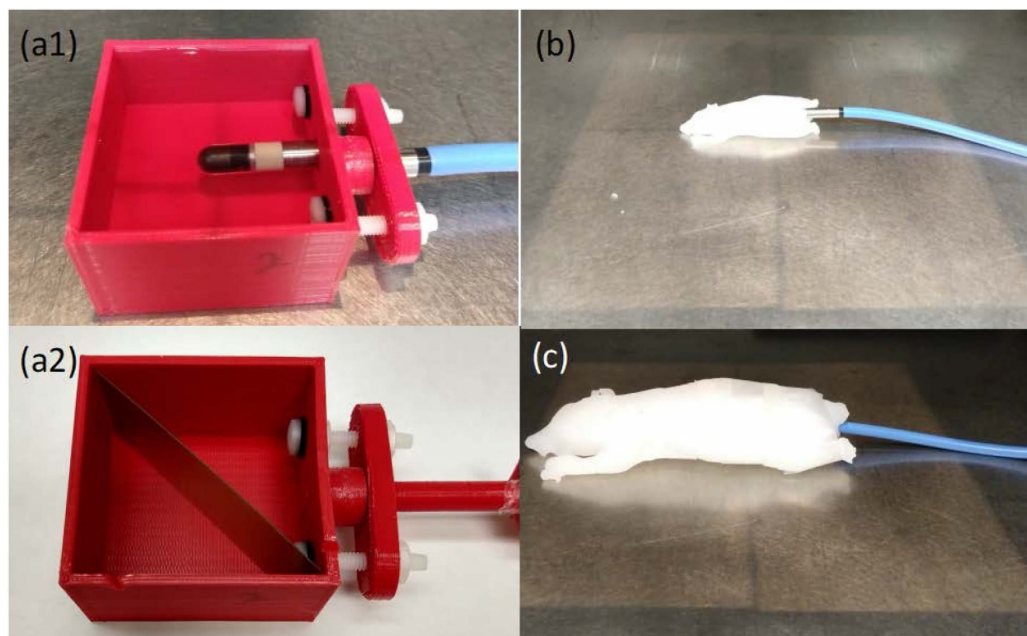


Figure 2. (a1)-(a2) Custom made small water tank with the sidewall opening for ionization chamber midplane dose measurements (a1) and a vertically inserted film for depth dose measurements (a2). (b) and (c) are photos of mouse and rat phantoms, respectively.

A $30.0 \times 30.0 \times 3.0 \text{ cm}^3$ solid water slab (Gammex Inc. Middleton, WI) with density of 1.04 g cm^{-3} was utilized as water equivalent phantom for the in-water dose rate measurements (figure 1(b)). The phantom consisted of a 2.0 cm thick slab, with a centrally drilled channel for ionization chamber placement, sandwiched between two 0.5 cm thick slabs. As a result, the ionization chamber was positioned at 1.5 cm below the top surface providing a midplane measurement point.

A small $5.0 \times 5.0 \times 3.2 \text{ cm}^3$ water phantom box was made from polylactic acid (PLA), a vegetable-based plastic material (MakerBot Industries LLC, New York, NY) using a 3D printing technique (figure 1(c)). The small phantom box was used to measure the in-water dose rate in an experimental setting representative of the small animal scale without full scatter conditions. The wall thickness of the box was 0.2 cm. Adding water to a 2.8 cm mark resulted in a 3.0 cm total water equivalent depth of the tank. A circular 7.0 mm diameter sidewall opening with a water sealing rubber washer was designed to mount an ionization chamber at the center of the phantom corresponding to a midplane measurement point. This small water phantom box was also used for the percent depth dose (PDD) measurements by vertically immersing a Gafchromic EBT3 film (Ashland Advanced Materials, Bridgewater, NJ) in water along the beam direction. A detailed structure of the small water tank is shown in figure 2.

In addition, to further mimic common experimental scenarios, mouse and rat rodentomorphic phantoms were made from EchoFlex 00–30 (Smooth-On Inc. Macungie, PA) with a density of 1.07 g cm^{-3} (figures 1(d) and (e)). A mold was 3D printed using a digital mouse phantom prototype from the CT data set in the 3D mouse atlas Digimouse (Dogdas *et al* 2007). The EchoFlex mixture was poured into the mold after degassing and cured for 24 h. A cylindrical hole with a 7 mm diameter was created in each phantom along the caudocranial direction for ionization chamber placement representative of a midplane measurement point.

Finally, midplane dose rate of a rodentomorphic mouse was measured for a whole-body mouse irradiation setup utilizing a mouse pie cage (Braintree Scientific Inc. Braintree, MA) (figure 1(f)). The diameter of the pie cage was 20.4 cm and the height was 5.6 cm. The thickness of the rotary cover and the bottom plate were 5.5 mm and 3.5 mm, respectively. The pie cage was divided into 11 sections and the thickness of the septum was 3.0 mm. One of the sections had twice the width of other sections, which was used to accommodate the mouse phantom and the ionization chamber during the measurements.

2.2. Whole-body dose rate measurements

2.2.1. In-air measurements for output calibration.

The in-air calibration was performed in accord with the AAPM TG-61 protocol. The 3 mm steel plate was removed from the cabinet during calibration and the Sun Nuclear 1D scanner was placed directly on the cabinet bottom floor (figure 1(a)). The position of the detector holder was adjusted such that the ionization chamber was set at a 65 cm focal spot distance (FSD), corresponding to the nominal position of the top surface of the steel plate. The motorized collimator was fully open, providing a $26.4 \times 26.4 \text{ cm}^2$ radiation field at 65 cm FSD. The ionization chamber was positioned at the center of the field.

ADCL calibrated PTW UNIDOS E electrometer and N31010 ionization chamber were utilized for dose rate measurements. The in-air method of the protocol was used to determine the absorbed dose rate to water, $\dot{D}_{w,cal}$, at the surface of a water phantom at a 65 cm FSD chosen as the calibration reference point. The energy of the x-ray was set to 250 kVp and the current was set to 15 mA. The irradiator exposure time was set to 15 min throughout the measurements and the cumulative charge readings were recorded for 1-min intervals. The average value over three measurements was used for each data point.

The absorbed dose to water, $D_{w,cal}$, for the calibration point at the surface of a semi-infinite water phantom with source-to-surface distance (SSD) of 65 cm ($SSD_{cal} = 65 \text{ cm}$) is given by

$$D_{w,cal} = MN_K B_W P_{stem,air} \left[\left(\frac{\bar{\mu}_{en}}{\rho} \right)_{air}^w \right]_{air}, \quad (1)$$

where M is the corrected in-air ionization chamber charge reading at the calibration point incorporating the correction for temperature, pressure, ion recombination, polarity effect and the electrometer calibration coefficient; N_K is the ionization chamber air-kerma calibration coefficient; B_W is the backscatter factor; $P_{stem,air}$ is the chamber stem correction factor; and $\left[\left(\frac{\bar{\mu}_{en}}{\rho} \right)_{air}^w \right]_{air}$ is the water-to-air ratio of the mean mass energy-absorption coefficients averaged over the incident photon spectrum. The calculated dose $D_{w,cal}$ was divided by the 1 min time interval to yield the dose rate to water $\dot{D}_{w,cal}$.

2.2.2. In-water measurements: solid water phantom.

After in-air calibration, the steel plate was placed back into the irradiator at its fixed position of 65 cm relative to the x-ray focal spot. The solid water phantom $30.0 \times 30.0 \times 3.0 \text{ cm}^3$ was placed directly on top of the plate (figure 1(b)). The ionization chamber was inserted into the drilled chamber channel at a midplane point 1.5 cm below the surface. Therefore, the dose rate was measured in phantom placed at a 62 cm SSD along with the ionization chamber at a 63.5 cm FSD. The electrometer readings were averaged over three 1 min charge collection intervals. The x-ray collimator jaws were fully open creating a $26.4 \times 26.4 \text{ cm}^2$ field at the plate surface.

The in-water absorbed dose to water at a depth z below the surface is given by

$$D_{w,z} = MN_K P_{Q, cham} P_{sheath} \left[\left(\frac{\bar{\mu}_{en}}{\rho} \right)_{air}^w \right]_w, \quad (2)$$

where M is the corrected ionization chamber reading; N_K is the ionization chamber air-kerma calibration coefficient from the ADCL calibration report; $P_{Q, cham}$ represents overall correction factor accounting for the change in beam quality between calibration and measurement and perturbation of the photon fluence at the point of measurement by the chamber and the chamber stem, and it was set to unity; P_{sheath} is waterproofing sheath correction factor if present, which was set to unity as a sheath was not used; and $\left[\left(\frac{\bar{\mu}_{en}}{\rho} \right)_{air}^w \right]_w$ is the water-to-air ratio of the mean mass energy-absorption coefficients at the reference point in water obtained

from Table VII in TG-61 protocol (Ma *et al* 2001). The dose rate $\dot{D}_{w,z}$ was determined by dividing $D_{w,z}$ by the 1 min charge collection time interval.

2.2.3. In-water measurements: small water phantom box.

The setup for the in-water dose rate measurements utilizing the small $5.0 \times 5.0 \times 3.2 \text{ cm}^3$ water phantom box, shown in figure 1(c), was analogous to the solid-water slab phantom. The water phantom box was placed on top of the steel plate. The phantom and the collimator beam center were aligned using the light field crosshair feature. The ionization chamber was inserted at a 1.5 cm depth corresponding to the center of the phantom and a midplane measurement point which was at a 63.5 cm from the x-ray tube focal spot. The box was filled with water to a 2.8 cm mark, resulting in a 3 cm water equivalent phantom thickness. This setup has the same height as the $30.0 \times 30.0 \times 3.0 \text{ cm}^3$ solid water phantom in figure 1(b), however, with considerably less scatter volume due to decreased lateral dimensions of the phantom. The in-water absorbed dose was determined by using equation (2) and dose rate was determined by dividing the dose by the time interval.

In addition, the water phantom was also used for the measurement of PDD curve. A $6.5 \times 2.8 \text{ cm}^2$ EBT3 film was inserted vertically into the small water phantom box along the diagonal direction. The box was filled with water to the top edge of the film. The center of the film was aligned to the beam center. Two films were irradiated for 180 s at a 250 kVp tube potential and 15 mAs tube current. The films were scanned using an Epson 10000XL flatbed scanner (Epson America Inc. Long Beach, CA) 24 h after the exposure. The optical densities were converted to dose using a previously created calibration curve which provided the depth dose curve. The depth dose curve was normalized by the dose at d_{max} to obtain the corresponding PDD values.

2.2.4. In-medium measurements: rodentomorphic mouse and rat phantoms.

The in-medium dose rate measurements were conducted utilizing rodentomorphic mouse and rat phantoms. Each phantom was placed on top of the steel plate with the body center aligned to the beam center (figures 1(c) and (d)). The ionization chamber was inserted at a midplane measurement point for both phantoms (figures 2(b) and (c)). The SSDs and the ionization chamber depths were different from the values in the water box phantom due to rodentomorphic form and size variations between mouse and rat phantoms. The SSDs of the mouse and rat phantoms were 62.9 cm and 61.5 cm, respectively, and the midplane ionization chamber depths were 1.05 cm and 1.75 cm, respectively. The measurements were conducted following the TG-61 protocol for the in-medium scenario. The doses were calculated using equation (2) and the dose rates were determined by dividing the doses by the time interval.

2.2.5. In-medium measurements: mouse phantom in a mouse pie cage.

Finally, the pie cage was placed on top of the steel plate and the mouse phantom was placed inside the largest compartment of the pie cage. The ionization chamber was inserted at a midplane measurement point within the mouse phantom. The mouse pie cage was positioned with its center aligned with the center of the field on the steel plate (figure 1(e)). The mouse phantom SSD was 62.0 cm and the midplane measurement depth was 1.05 cm. The in-medium absorbed dose rate measurements were performed in accord with the TG-61 formalism and the dose was calculated using equation (2). The dose rate was calculated by dividing the dose by the time interval.

The summary of all measurements described in this section is provided in table 1.

2.3. Monte Carlo simulations

The Geant4 Application for Tomographic Emission (GATE, version 8.1) (Agostinelli *et al* 2003, Jan *et al* 2004) was used to compute absorbed dose distributions inside the designed phantoms via the Monte Carlo (MC) simulation method. A physics list `emstandard_opt3` was used as suggested by Geant4 manual for simulations requiring high dosimetric accuracy. The track length estimator method (Williamson 1987) was employed for fast dose calculation. The x-ray tube was treated as an isotropic point source emitting photons in a cone with a 16° half angle. The photon energies were sampled from a 250 kVp x-ray spectrum, which was calculated using SpekCalc (Poludniowski *et al* 2009) with the electron incident angle of 30° and an extra 1.35 mm thick Al filtration, yielding the same HVL as the experimental value of 0.45 mm Cu. The x-ray beam was collimated with a 1.90 cm thick Pb square opening to produce a $26.4 \times 26.4 \text{ cm}^2$ field at 65 cm from the source.

The simulated geometries were identical to the phantom geometries used in the experiments. The focal point of the source, the center of the collimator and the center of phantoms were aligned along the vertical axis. A total of 10^{10} photons were simulated for each case resulting in less than 0.5% relative dose uncertainty. Each simulation was split into four tasks that were distributed to four individual CPU cores to further speed up the calculations.

Table 1. Summary of experimental geometries used for ionization chamber measurements.

Ionization chamber measurements	Description	Phantom dimensions [cm ³]	SSD [cm]	Measurement depth [cm]
IC-1	In air calibration	NA	65.0 FSD	NA
IC-2	Solid water phantom	30.0 × 30.0 × 3.0	62.0	1.5
IC-3	Small water box	5.0 × 5.0 × 3.0	62.0	1.5
IC-4	Mouse phantom	3.8 × 10.0 × 2.1	62.9	1.05
IC-5	Rat phantom	8.0 × 21.0 × 3.5	61.5	1.75
IC-6	Mouse phantom in a pie cage	3.8 × 10.0 × 2.1 (mouse phantom only)	62.0	1.05

The reference simulation was performed for the in-air calibration setup, MC-1 simulation in table 2. The center of an 1.0 mm³ water voxel was placed at 65.0 cm from the x-ray source. Dose calculation was performed yielding dose to water at the center of the voxel. The number was further corrected for the attenuation by the 0.5 mm water above the center of the voxel to generate $\dot{D}_{MC,ref}$ in the unit of Gy/photon. Denote the ionization chamber measured dose rate to water at this point by $\dot{D}_{IC,ref}$ in the unit of Gy/min. $\dot{D}_{IC,ref}$ was measured following the procedure described in section 2.2.1 and calculated using eq. (1). Next, the calibration factor $f = \dot{D}_{IC,ref}/\dot{D}_{MC,ref}$ was computed in the unit of photon/min. This factor was applied to all subsequent MC dose calculation cases, which facilitated the comparison between calculated and experimentally measured dose values.

An extra simulation was performed in support of the MC model authentication. Namely, dose at the surface of a large 30.0 × 30.0 × 27.0 cm³ water phantom at a 65.0 cm from the x-ray focal spot was computed. This step enabled determination of the backscatter factor B_W under full scatter condition. The computed B_W value was then compared with published data (Ma *et al* 2001) which served as validation for the MC dose calculation model.

After that, the simulations were performed for the measurement geometry configurations and materials given in table 1, with the corresponding computational details listed in table 2. Specifically, for the MC-2 simulation, the steel plate was simulated as material SS304 included in the GATE database, and a 30.0 × 30.0 × 3.0 cm³ solid water phantom was placed on top of the plate at a 62 cm SSD. This configuration matched the IC-2 measurement setup described in section 2.2.2. Pure water was used as the phantom material because of the unknown specific material composition of the solid water. Correspondingly, for the IC-3 measurement described in section 2.2.3, the MC-3 simulation computed dose in a small 5.0 × 5.0 × 3.0 cm³ water phantom placed on top of the steel plate. Similarly, digital mouse and rat phantoms simulations, MC-4 and MC-5, respectively, corresponded to the measurements described in section 2.2.4. The digital phantoms were generated from CT data set in the 3D mouse atlas Digimouse (Dogdas *et al* 2007), and the density was overridden to that of the EchoFlex material $\rho = 1.07$ g/cm³. The assigned material was pure water because of the unknown specific compositions of EchoFlex. Lastly, the MC-6 simulation was performed for the setup with the mouse phantom placed inside the pie cage identical to the geometry in the experiment. A geometry model of the pie cage was constructed based on published blueprints, and the material was set to Polymethyl methacrylate (PMMA) with a density of $\rho = 1.18$ g/cm³. In all cases, the simulations yielded 3D dose distributions throughout the phantoms. Point doses at the position corresponding to the measurement points were extracted.

2.4. Point dose calculations

It is of great importance to understand the agreement, or disagreement, between the true dose rate in a specific experiment and the value calculated using hand calculations based on lookup tables. The assessment of the accuracy of hand calculations commonly used in preclinical radiobiology studies is mostly overlooked. For the TBI experiment in this study, the dose rate at the prescription point can be calculated as following. Based on the calibrated irradiator output, $\dot{D}_{w,cal}$, the dose rate at the reference point, $\dot{D}_{w,0}$, at the surface of an animal, is calculated using

$$\dot{D}_{w,0} = \dot{D}_{w,cal} \left(\frac{SSD_{cal}}{SSD} \right)^2, \quad (3)$$

where SSD_{cal} and SSD stand for the calibration point distance and the animal surface distance relative to the x-ray focal spot, respectively. Based on the XRad 320 design, a 62 cm SSD is typically used for a standard whole-body irradiation setup, as the animal is placed on the steel plate and a 3 cm thickness of the animal is assumed.

Table 2. Summary of geometries and materials in MC simulations.

MC run	Setup description	Phantom dimensions [cm ³]	Phantom material	Voxel size [cm ³]	SSD [cm]	Depth [cm]
MC-1	In-air calibration	0.1 × 0.1 × 0.1	Water	0.1 × 0.1 × 0.1	64.95	NA
MC-2	Solid water phantom	30.0 × 30.0 × 3.0	Water	0.5 × 0.5 × 0.1	62.0	1.5
MC-3	Small water box	5.0 × 5.0 × 3.0	Water	0.5 × 0.5 × 0.1	62.0	1.5
MC-4	Mouse phantom	3.8 × 10.0 × 2.1	Water	0.1 × 0.1 × 0.1	62.9	1.05
MC-5	Rat phantom	8.0 × 21.0 × 3.5	Water	0.1 × 0.1 × 0.1	61.5	1.75
MC-6	Mouse phantom in a pie cage	3.8 × 10.0 × 2.1 (mouse phantom only)	Water	0.1 × 0.1 × 0.1	62.0	1.05

Table 3. Measured $\dot{D}_{W,IC}$ and MC simulation $\dot{D}_{W,MC}$ dose rate results in different phantoms.

IC & MC	Setup description	SSD [cm]	Measurement depth [cm]	$\dot{D}_{W,IC}$ [Gy/min]	$\dot{D}_{W,MC}$ [Gy/min]	e [%]
IC-1 & MC-1	In-air calibration	65.0 FSD	NA	1.537	1.537	0.0 (by definition)
IC-2 & MC-2	Solid water phantom	62.0	1.5	1.314	1.349	2.6
IC-3 & MC-3	Small water box	62.0	1.5	1.155	1.166	0.9
IC-4 & MC-4	Mouse phantom	62.9	1.05	1.070	1.106	3.3
IC-5 & MC-5	Rat phantom	61.5	1.75	0.976	1.014	3.9
IC-6 & MC-6	Mouse phantom in a pie cage	62.0	1.05	1.105	1.114	0.8

The dose rate at the targeted midplane point 1.5 cm below the surface is a product of the dose rate at the reference point and the *PDD* value at 1.5 cm depth,

$$\dot{D}_{w,z=1.5} = \dot{D}_{w,0} * PDD(1.5) / 100. \quad (4)$$

The *PDD* values were measured using the small water phantom box (figure 1(c)) by utilizing an EBT3 film.

3. Results

3.1. Experimental results

The measured dose rates are listed in table 3. For the in-air method, the dose rate at a 65.0 cm FSD calibration point was 1.537 Gy min⁻¹. The in-water midplane dose rate measured at 1.5 cm depth below the surface of the 30.0 × 30.0 × 3.0 cm³ solid water phantom slab was 1.314 Gy min⁻¹. The next measurement with the identical setup, however, utilizing the small 5.0 × 5.0 × 3.0 cm³ water phantom box, yielded the in-water midplane dose rate of 1.155 Gy min⁻¹. The reduction in dose rate can be attributed to reduced lateral x-ray scatter caused by the small phantom size. For rodentomorphic phantoms, the mouse and rat measured in-water midplane dose rates were 1.07 Gy min⁻¹ and 0.976 Gy min⁻¹, respectively. Lastly, the measured in-water midplane dose rate for a mouse phantom placed inside the pie cage was 1.105 Gy min⁻¹.

The depth dose distribution along the central incident beam path in the small water box was read out from the EBT3 film. The corresponding *PDD* values were calculated by normalizing the depth dose curve to the maximum dose. The results are shown in figure 3. The *PDD* at 1.5 cm depth was 84.1% for the small water box.

3.2. Monte Carlo simulation results

The reference simulation MC-1, yielded a dose value of $\dot{D}_{MC,ref} = 4.475 \times 10^{-10}$ Gy/photon, which established a calibration factor of $f = 2.346 \times 10^{15}$ photon/min. This factor was used to convert MC calculated values to the actual dose rate values in all subsequent cases.

The added simulation, which served as the MC model validation, computed a dose rate of 1.517 Gy min⁻¹ at the surface of a semi-infinite water phantom under a full scatter condition. In turn, a backscatter factor of $B_W = 1.448$ was obtained. This value agreed favorably with the published result of $B_{W,TG-61} = 1.493$ in table V of the AAPM TG-61 report (Ma *et al* 2001). Considering the uncertainties of published B_W values and the use of equivalent FS (square field in our study and circular fields in TG-61), the 3% relative difference between $B_{W,TG-61}$ and B_W was acceptable and was considered to confirm the validity of the utilized MC model.

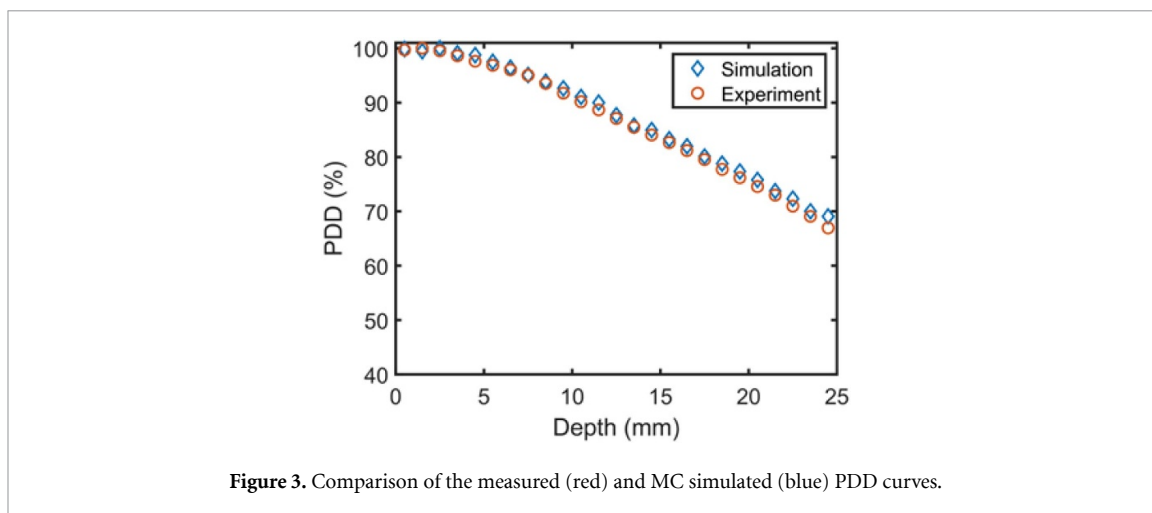


Figure 3. Comparison of the measured (red) and MC simulated (blue) PDD curves.

Table 4. Relative dose rate differences calculated using the point dose hand calculation method compared to the ionization chamber measurements and MC simulations.

IC & MC	Setup description	$\Delta\dot{D}_{IC}$ [%]	$\Delta\dot{D}_{MC}$ [%]	$\frac{1}{2} [\Delta\dot{D}_{IC} + \Delta\dot{D}_{MC}]$ [%]
IC-2 & MC-2	Solid water phantom	15.0	16.7	15.9
IC-3 & MC-3	Small water box	25.3	28.0	26.7
IC-4 & MC-4	Mouse phantom	30.8	31.7	31.3
IC-5 & MC-5	Rat phantom	36.9	36.0	36.5
IC-6 & MC-6	Mouse phantom in a pie cage	28.5	31.2	29.9

The dose rate values at the points of interest corresponding to the measurement points in various phantom configurations are summarized in table 3. Overall, the MC calculated dose rates were in good agreement with the measured dose rates. The relative dose rate difference $e = |\dot{D}_{w,IC} - \dot{D}_{w,MC}| / \dot{D}_{w,IC}$ was 2.6% and 0.9% for the solid water and small water box, respectively. The difference was found to be somewhat larger for the mouse phantom, the rat phantom, and the mouse phantom in the pie cage scenarios, 3.3%, 3.9%, and 0.8%, respectively. This was attributed to the uncertainties in geometry, such as phantom setup and chamber placement, as well as to the unknown phantom material composition which was simulated as water for the mouse and rat phantoms. The PDD in small water box phantom computed by MC simulation is plotted in figure 3. The computed PDD generally agreed well with PDD measured using a film, and the average difference between the two curves was 0.74%. The relative difference between MC and measured PDD at 1.5 cm depth was 0.9% for the small water box.

3.3. Comparison with point dose using a hand calculation method

The lookup tables and hand calculation methods for a given radiation quality and SSD, e.g. Section 2.4., generally account for backscatter as a function of FS. However, such an approach is not setup specific and disregards variations in phantom dimensions. Based on this approach, the calculated dose rate was $\dot{D}_{w,z=1.5} = 1.546$ Gy/min, independent of phantom size. Yet, the ionization chamber measurements and MC simulations revealed that the setup variations result in large dose rate differences as the backscatter factor can dramatically change for two similar experimental arrangements. The difference between the actual dose rate and the value using hand calculations was computed as $\Delta\dot{D}_i = (\dot{D}_{w,z=1.5} - \dot{D}_{w,i}) / \dot{D}_{w,i}$, where $i = IC, MC$ stands for ionization chamber and MC methods, respectively. The relative dose rate differences with respect to the measurement and the simulation, as well as the average of the two, are summarized in table 4.

In all the scenarios examined in this study, the point dose hand calculation approach overestimated dose rates, the relative difference spanned from $\sim 16\%$ to 37% , when taking the average of ΔD_{IC} and ΔD_{MC} . Note that the irradiator was initially calibrated following the in-air TG-61 procedure and that the 3 mm steel plate was removed to facilitate the calibration. For all subsequent setups, the steel plate was put back to support phantom measurements. Apparently, the steel plate did not provide sufficient backscatter relative to the in-air reference condition, yielding the observed dose rate overestimation for hand calculations. The 16% overestimation for the solid water phantom increased to 27% for the small water box, which can be ascribed to the reduction of the lateral photon scattering. For rodentomorphic phantoms, the overestimation was further amplified from 31% for the mouse to 36% for the rat phantom. In general, the overestimation was larger for smaller phantoms due to reduced phantom dimensions. This was not the case when comparing the

rat with the mouse phantom. While the rat phantom was able to provide more scattered photons relative to the mouse phantom, the measurement points were at 1.75 cm and 1.05 cm, respectively. This was different than the assumed 1.5 cm depth for hand dose calculation and it represented the largest contribution to the dose rate discrepancies.

4. Discussion and conclusions

In a TBI setup, a single large field x-ray beam is encompassing the entire body of the animal (rats or mice). The exposure time needed to deliver a prescribed dose to an animal midplane point is calculated based on the x-ray beam calibration in a reference condition following an established protocol, e.g. the AAPM TG-61. It is important to point out that the calibration procedures and underlining data for the reference dosimetry protocols generally assume full photon scattering conditions, including sufficient lateral scatter in the irradiated volume and backscatter beyond the point of irradiation. This assumption is often not satisfied in preclinical experimental settings due to the small animal size and the irradiator design.

Specifically, in this study, TBI dose rates for several phantom configurations were measured and computed using MC simulations. While the ionization chamber measurements and MC computed dose rates closely agreed within 3.9% (table 3), the dose rate variations were an order of magnitude larger when commonly used lookup tables and hand dose calculation methods were used (table 4). The results of the study determined that the steel plate, which is an integral part of the irradiator's design, does not provide sufficient photon backscatter relative to the reference in-air calibration condition, yielding overestimated dose rate values. The lack of lateral scatter due to relatively small phantom size further exacerbated this issue. These findings demonstrate the necessity for setup-specific measurements and sophisticated dose calculation methods to provide accurate dosimetry for preclinical experiments.

One possible solution to this problem could be the implementation of a fast MC simulation system together with a digital animal phantom to allow real-time setup-specific dose calculations. GPU-based fast MC dose calculation tools have been developed in recent years (Jia *et al* 2010, 2011, 2012, 2014). It is our ongoing work to build a new and accurate dose calculation system using these tools to support preclinical radiobiology studies.

In a recent paper (Gronberg *et al* 2020), regarding preclinical dosimetry verification utilizing a mail audit system, the audit results agreed much better with the MC calculations than the table-based calculations. The authors' reasoning was that MC calculations incorporate the necessary scatter conditions of the employed phantom which is only approximated by just using dosimetry data lookup tables.

The measurements for all experimental geometries were performed in accord with the TG-61 in-air or in-phantom methods. The estimated combined standard uncertainty for $\dot{D}_{W,IC}$ for both in-air and in-phantom methods was $\pm 4.7\%$, see Table III in TG-61 document. The corresponding uncertainty for $\dot{D}_{W,MC}$ utilizing MC simulations was $\pm 0.5\%$. On average, the relative dose rate difference for all cases was 2.3%, spanning from 0.9% to 3.9%. Therefore, the measured and simulated results agreed within the corresponding error bar intervals.

The ionization chamber used for measurements was calibrated in-air in terms of air kerma for the UW250-M beam quality. However, the choice of beam quality is not always straightforward, as the ADCL calibration conditions may not be identical to the user's irradiator specifications. The ADCL beam codes or beam qualities are stratified based on the inherent filtration (mm Be), the tube voltage (kVp), the additional filtration (mm Al or Cu) and the HVL layer (mm Al or Cu). The x-ray tube inherent filtration of 3 mm Be, the manufacturer's choice of 1.65 mm Al added filtration, the measured HVL of 0.45 mm Cu and the intended 250 kVp tube potential made it difficult to choose the adequate ADCL beam code. Based on these values, the ADCL defined calibration conditions were not a perfect match for the irradiator regardless of the beam code selection. Ultimately, the UW250-M beam quality was chosen and the corresponding air kerma calibration coefficient was used without any interpolations. To justify the UW250-M beam quality selection, the output of the system was independently verified. The ratio of stated versus measured dose was 1.01, using lithium fluoride TLD measurements read by the Radiation Dosimetry Services at MD Anderson Cancer Center in Houston TX. These results were reported in a previous manuscript published by our group (Pidikiti *et al* 2011).

In conclusion, this study outlined comprehensive investigational efforts to accurately determine dose rate for TBI experiments, a classical preclinical radiobiology and immunology research method. It was found that small changes in the TBI experimental setup could result in large dose rate variations. The traditional hand calculation method to determine dose is likely to overestimate the dose, sometimes to a substantial extent. MC simulations and the corresponding measurements specific to a designed experimental setup are vital for accurate preclinical dosimetry and reproducibility of radiobiological findings.

The initial motivation for this study was quality assurance after a service call and repair of the irradiator. The in-air irradiator calibration was confirmed but an additional phantom measurement did not agree with a basic hand calculation. This puzzle was unraveled only after the series of additional measurements and MC simulations presented in this work. The take home message is that even the seemingly simple whole-body irradiation format entails physics expertise essential for reliable and repeatable biological experiments. This study supports the well-recognized concern for small animal irradiation dosimetry errors and highlights the need for physics consultation even in what is considered to be simple, straightforward dosimetry determinations.

Acknowledgments

This work is supported in part by grants from the National Institutes of Health (R37CA214639) and from the Core Facility Award (RP180770) from the Cancer Prevention Research Institute of Texas.

ORCID iD

Strahinja Stojadinovic  <https://orcid.org/0000-0002-6840-5747>

References

- Agostinelli S et al 2003 GEANT4—a simulation toolkit *Nucl. Instrum. Methods Phys. Res. A* **506** 250–303
- Chow J C L, Leung M K K, Lindsay P E and Jaffray D A 2010 Dosimetric variation due to the photon beam energy in the small-animal irradiation: a Monte Carlo study *Med. Phys.* **37** 5322–9
- Clarkson R, Lindsay P E, Ansell S, Wilson G, Jelveh S, Hill R P and Jaffray D A 2011 Characterization of image quality and image-guidance performance of a preclinical microirradiator *Med. Phys.* **38** 845–56
- Deng H, Kennedy C W, Armour E, Tryggestad E, Ford E, McNutt T, Jiang L and Wong J 2007 The small-animal radiation research platform (SARRP): dosimetry of a focused lens system *Phys. Med. Biol.* **52** 2729–40
- Desrosiers M, Dewerd L, Deye J, Lindsay P, Murphy M K, Mitch M, Macchiarini F, Stojadinovic S and Stone H 2013 The importance of dosimetry standardization in radiobiology *J. Res. Natl Inst. Stand. Technol.* **118** 16
- Dogdas B, Stout D, Chatziioannou A F and Leahy R M 2007 Digimouse: a 3D whole body mouse atlas from CT and cryosection data *Phys. Med. Biol.* **52** 577–87
- Draeger E, Sawant A, Johnstone C, Koger B, Becker S, Vujaskovic Z, Jackson I L and Poirier Y 2020 A dose of reality: how 20 years of incomplete physics and dosimetry reporting in radiobiology studies may have contributed to the reproducibility crisis *Int. J. Radiat. Oncol. Biol. Phys.* **106** 243–52
- Gronberg M P, Tailor R C, Smith S A, Kry S F, Followill D S, Stojadinovic S, Niedzielski J S, Lindsay P E, Krishnan S and Aguirre F 2020 A mail audit independent peer review system for dosimetry verification of a small animal irradiator *Radiat. Res.* **193** 341–50
- Jan S et al 2004 GATE: a simulation toolkit for PET and SPECT *Phys. Med. Biol.* **49** 4543–61
- Jia X, Gu X, Graves Y J, Folkerts M and Jiang S B 2011 GPU-based fast Monte Carlo simulation for radiotherapy dose calculation *Phys. Med. Biol.* **56** 7017–31
- Jia X, Gu X, Sempau J, Choi D, Majumdar A and Jiang S B 2010 Development of a GPU-based Monte Carlo dose calculation code for coupled electron-photon transport *Phys. Med. Biol.* **55** 3077
- Jia X, Yan H, Gu X and Jiang S B 2012 Fast Monte Carlo simulation for patient-specific CT/CBCT imaging dose calculation *Phys. Med. Biol.* **57** 577–90
- Jia X, Ziegenhein P and Jiang S B 2014 GPU-based high-performance computing for radiation therapy *Phys. Med. Biol.* **59** R151
- Lindsay P E et al 2014 Multi-institutional dosimetric and geometric commissioning of image-guided small animal irradiators *Med. Phys.* **41** 12
- Ma C M, Coffey C W, Dewerd L A, Liu C, Nath R, Seltzer S M and Seuntjens J P 2001 AAPM protocol for 40–300 kV x-ray beam dosimetry in radiotherapy and radiobiology *Med. Phys.* **28** 868–93
- Na Y H, Wang Y F, Black P J, Velten C, Qian X, Lin S C, Adamovics J and Wu C S 2018 Dosimetric and geometric characteristics of a small animal image-guided irradiator using 3D dosimetry/optical CT scanner *Med. Phys.* **45** 3330–9
- Newton J, Oldham M, Thomas A, Li Y F, Adamovics J, Kirsch D G and Das S 2011 Commissioning a small-field biological irradiator using point, 2D, and 3D dosimetry techniques *Med. Phys.* **38** 6754–62
- Noblet C, Chiavassa S, Smekens F, Sarrut D, Passal V, Suhard J, Lisbona A, Paris F and Delpon G 2016 Validation of fast Monte Carlo dose calculation in small animal radiotherapy with EBT3 radiochromic films. *Phys. Med. Biol.* **61** 3521
- Pedersen K H, Kunugi K A, Hammer C G, Culbertson W S and Dewerd L A 2016 Radiation biology irradiator dose verification survey *Radiat. Res.* **185** 163–8
- Pidikiti R, Stojadinovic S, Speiser M, Song K H, Hager F, Saha D and Solberg T D 2011 Dosimetric characterization of an image-guided stereotactic small animal irradiator *Phys. Med. Biol.* **56** 2585–99
- Poludniowski G, Landry G, Deblois F, Evans P M and Verhaegen F 2009 SpekCalc: a program to calculate photon spectra from tungsten anode x-ray tubes *Phys. Med. Biol.* **54** N433–N438
- Seed T M et al 2016 An interlaboratory comparison of dosimetry for a multi-institutional radiobiological research project: observations, problems, solutions and lessons learned *Int. J. Radiat. Biol.* **92** 59–70
- Soultanidis G et al 2019 Development of an anatomically correct mouse phantom for dosimetry measurement in small animal radiotherapy research *Phys. Med. Biol.* **64** 12NT02
- Tryggestad E, Armour M, Iordachita I, Verhaegen F and Wong J W 2009 A comprehensive system for dosimetric commissioning and Monte Carlo validation for the small animal radiation research platform *Phys. Med. Biol.* **54** 5341–57
- van Hoof S J, Granton P V and Verhaegen F 2013 Development and validation of a treatment planning system for small animal radiotherapy: smART-Plan *Radiother. Oncol.* **109** 361–6

- Vaniqui A, Walters B R, Fonseca G P and Verhaegen F 2019 Dose to water versus dose to medium from cavity theory applied to small animal irradiation with kilovolt x-rays *Phys. Med. Biol.* **64** 165001
- Williamson J F 1987 Monte Carlo evaluation of kerma at a point for photon transport problems *Med. Phys.* **14** 567–76
- Wong J *et al* 2008 High-resolution, small animal radiation research platform with x-ray tomographic guidance capabilities *Int. J. Radiat. Oncol. Biol. Phys.* **71** 1591–9
- Yoshizumi T, Brady S L, Robbins M E and Bourland J D 2011 Specific issues in small animal dosimetry and irradiator calibration *Int. J. Radiat. Biol.* **87** 1001–10